

Coexistence of Zonal Flows and Drift-Waves in a Cylindrical Magnetized Plasma

Yoshihiko NAGASHIMA*, Sanae-I. ITOH, Shunjiro SHINOHARA¹, Masayuki FUKAO²,
Akihide FUJISAWA³, Kenichiro TERASAKA¹, Yoshinobu KAWAI, Naohiro KASUYA³,
George R. TYNAN⁴, Patrick H. DIAMOND⁵, Masatoshi YAGI,
Shigeru INAGAKI, Takuma YAMADA⁶, and Kimitaka ITOH³

Research Institute for Applied Mechanics, Kyushu University, Kasuga, Fukuoka 816-8580

¹*Interdisciplinary Graduate School of Engineering Science, Kyushu University, Kasuga, Fukuoka 816-8580*

²*Uji, Kyoto 611-001*

³*National Institute for Fusion Science, Toki, Gifu 509-5292*

⁴*Center for Energy Research, University of California, San Diego, La Jolla, CA 92093-0417, U.S.A.*

⁵*Center for Astrophysics and Space Sciences, University of California, San Diego, La Jolla, CA 92093-0424, U.S.A.*

⁶*Graduate School of Frontier Science, University of Tokyo, Kashiwa, Chiba 509-5292*

(Received February 5, 2008; accepted August 11, 2008; published October 27, 2008)

Spatiotemporal structures of fluctuations with frequencies lower than the ion cyclotron frequency in a cylindrical magnetized plasma are investigated. Drift-wave and low-frequency zonal flow coexist. Electrostatic potentials of the zonal flow and the drift-wave are distributed widely in radius. The radial wave number profile of the zonal flow has a shear structure at the radial location where the drift-wave has a maximal normalized fluctuation amplitude. On the other hand, the radial wave number profile of the drift-wave shows vortex tilting, resulting in the generation of stationary turbulence Reynolds stress gradient per mass density. The envelope and bispectral analyses indicate significant nonlinear interactions between the zonal flow and the drift-wave.

KEYWORDS: turbulence, drift-wave, zonal flow, linear magnetized plasma, envelope analysis, bispectral analysis
DOI: [10.1143/JPSJ.77.114501](https://doi.org/10.1143/JPSJ.77.114501)

1. Introduction

Drift-wave instability is a universal phenomenon in magnetized plasmas with a spatial pressure gradient. It is recognized that drift-wave turbulence dominates over the edge plasma turbulence of magnetically confined fusion plasmas and contributes markedly to the anomalous transport of particles, heat and momentum.¹⁾ Many laboratory linear and toroidal plasma experiments have been conducted in order to understand the basic physics of drift-wave turbulence.^{2–13)} The progress of these studies clarified that drift-wave turbulence includes not only linearly unstable fluctuations but also nonlinearly excited quasi-modes with various spatiotemporal structures. Zonal flows, azimuthally symmetric bandlike shear flows, are an example of quasi-modes and are universally observed in nature and laboratories.^{14–16)} Zonal flows are linearly stable and are exclusively driven by the nonlinearity of drift-wave turbulence (the drift wave-zonal flow system). In addition, the back interaction of zonal flows can reduce turbulence and turbulent transport via the shearing effect,¹⁷⁾ and the existence of zonal flows affects turbulence levels and turbulent transport. Thus, experimental studies of zonal flows have been conducted intensively in toroidal fusion plasma research,^{18–25)} as well as a zonal magnetic field.²⁶⁾ Zonal flows were also found in basic linear plasmas.^{27,28)} In the controlled Shear decorrelation experiment (CSDX) device, the estimation of radial force balance identified that the turbulence Reynolds stress can maintain a steady state zonal flow. To understand mechanisms of turbulence including zonal flows in detail and to control plasma turbulence, the progress of research on the coexistence of drift-waves and zonal flows is crucial.

In this article, we present an experimental observation of the coexistence of a zonal flow with a finite frequency (~ 0.4 kHz) and a drift-wave spectrum (7–8 kHz and its higher harmonics) in a cylindrical laboratory plasma. In this observation, the zonal flow has a finite frequency. We focus mainly on details of spatiotemporal structures of fluctuations in this paper. The content of this manuscript is as follows. First, we describe experimental conditions. Next, we show a general introduction of observed fluctuations. Third, specific topics are given. Slices of normalized auto-power spectra in frequency and in radius discriminate fluctuations in terms of the Boltzmann relationship. Poloidal, axial, and radial wave numbers are derived by cross-phase analysis. In addition, results from a time delay estimation analysis confirm that the electrostatic potential of the residual zonal flow is associated with a poloidal velocity fluctuation. On the other hand, we compare the observed and theoretically obtained linear dispersion relationships of the drift-wave. Furthermore, the envelope and bispectral analyses present evidence of nonlinear interactions between the residual zonal flow and the drift-wave. Finally, we discuss the shear structure of the zonal flow observed in this experiment.

2. Experimental Apparatus

Experiments were conducted on a linear device, the large mirror device (LMD) of Kyushu University.²⁹⁾ Figure 1(a) shows a schematic view of the LMD. The LMD has a cylindrical vacuum vessel made of stainless steel, with an inner diameter of 0.445 m and an axial length of 1.7 m. At one end of the vessel, plasmas are produced in a quartz tube with an inner diameter of 0.095 m and an axial length of 0.4 m. A radio frequency electromagnetic wave (RF) source with a frequency of 7 MHz is used for plasma production in the quartz tube. The RF input power is fixed at 2 kW during

*E-mail: nagashi@riam.kyushu-u.ac.jp

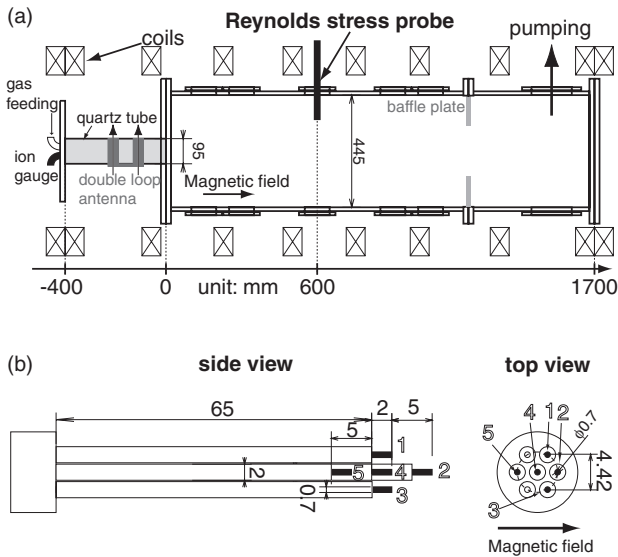


Fig. 1. Experimental devices. (a) Large mirror device. (b) Reynolds stress probe.

0.5 s discharge in these experiments. The RF antenna has a poloidal mode $m = 0$, and we estimate Helicon plasma production. The coexistence of the residual zonal flow and drift-wave spectrum is investigated under the following conditions. The magnetic field strength B is fixed at 0.12 T in the center of the vessel [$\omega_{ci}/(2\pi) \sim 46$ kHz]. Argon gas is fed at the end of the quartz tube, and the filling pressure $P_{Ar} = 0.44$ Pa is measured at the same location. Both ends of the cylindrical plasma production area are electrically connected to the vessel ground. The magnetic field is converging in the quartz tube and has a straight configuration in the vessel.

Under these experimental conditions, we reproducibly found that auto-power spectral forms change transiently from a combination of coherent peaks to a broadband feature during a single discharge with a constant magnetic field strength. In this manuscript, we focus our attention on fluctuations that keep stationary features during a single discharge. A study related to transient behaviors is also our interest in the viewpoint of the phase transition of fluctuations and will be presented in the future.

Fluctuations are mainly measured with a Reynolds stress probe (RSP) located 60 cm away from the end of the vessel (source side), shown in Fig. 1(b). The RSP head houses five electrodes for measuring five different locations in a poloidal cross section. The cylindrical electrodes with a diameter of 0.7 mm and a height of 2 mm are made of tungsten. The #4 electrode shown in Fig. 1(b) is used for the ion saturation current fluctuation measurement ($\tilde{I}_{i,sat}$) with a constant bias voltage (-70 V in the experiment). The other four electrodes are used for the floating potential fluctuation measurement ($\tilde{\Phi}_f$). Three Φ_f 's at #1, #2, and #3 electrodes ($\Phi_{f,1}$, $\Phi_{f,2}$, and $\Phi_{f,3}$) are used for measurements of the radial wave number k_r [the cross-phase between $(\Phi_{f,1} + \Phi_{f,3})/2$ and $\Phi_{f,2}$, 5 mm radial distance] and poloidal wave number k_θ (the cross-phase between $\Phi_{f,1}$ and $\Phi_{f,3}$, 4.4 mm poloidal distance). Poloidal velocity fluctuations \tilde{V}_θ are obtained by using time delay estimation (TDE).²⁷⁾ Signals are sampled by a 14-bit digitizer at a frequency of 1 MHz, combined with amplifiers

with an analog bandwidth of 100 kHz and with a signal time delay of less than 120 ns. (The phase delay is less than 0.5% in the frequency range lower than 50 kHz.) The equilibrium parameters (the electron temperature T_e and the electron density n_e) are also measured in separate discharges under the same operational conditions by sweeping the bias voltage at the #2 electrode. Normalized fluctuation amplitudes presented later were carefully checked in these equilibrium measurements. Other than the RSP, many Langmuir probes are installed azimuthally and axially at fixed locations for mode number measurements as well as for reference data. Unless stated in figures, the length of the data window for fast Fourier transform (FFT) is 16384. Error estimation is based on the statistical significance of spectral analysis and the variance in the number of discharges. Spectra are chosen at around 0.3 s from the beginning of discharges. Radial scans of the RSP with 0.5 cm intervals were performed to obtain radial profiles.

3. General Introduction of Observed Fluctuations

In this section, we show radial profiles of fluctuation spectra by which a general overview of fluctuations is introduced. Figures 2(a) and 2(b) show radial profiles of $\tilde{\Phi}_f/\overline{T_e}$ and $\tilde{I}_{i,sat}/\overline{I}_{i,sat}$ spectra, and distinctive four fluctuations are labeled. These two figures [Figs. 2(a) and 2(b)] are obtained by shot-to-shot radial scans of the RSP. To examine the spectral reproducibility of plasmas during a shot-to-shot scan, the spectrum of $\tilde{\Phi}_f$ obtained by a reference probe inserted from the bottom of the vessel ($z = 90$ cm) is shown in Fig. 2(c). In this experiment, the reference probe is fixed at the radial location $r = 4$ cm. A good spectral reproducibility is obtained in the radial range of 2–6.5 cm.

First, we focus on two distinctive fluctuations distributed in wide radial ranges. One is the fluctuation at 7–8 kHz, and the other is the fluctuation at 0.4 kHz. We denote the former or latter $\tilde{\Phi}_f$ fluctuation as the DW (drift-wave) or ZF (zonal flow), respectively. Confirmations are explained in the following sections sequentially. The DW is detected in both $\tilde{\Phi}_f/\overline{T_e}$ and $\tilde{I}_{i,sat}/\overline{I}_{i,sat}$, and the normalized fluctuation amplitudes are similar. In contrast to the DW, the $\tilde{\Phi}_f/\overline{T_e}$ of the ZF is dominant relative to $\tilde{I}_{i,sat}/\overline{I}_{i,sat}$. The DW and ZF are main topics in this paper. Meanwhile, we can see broadband fluctuations in the frequency range $f < 2$ kHz at the radial location $r > 4.5$ cm (denoted as EO, edge oscillation). The plasma radius is ~ 5 cm, determined by the diameter of the quartz tube, and the EO is located outside main plasmas. The spectral peak frequency of the EO is similar to that of the ZF. However, the EO has many higher harmonics, while the ZF has no clear higher harmonics. In addition, normalized powers of the EO are similar between $\tilde{\Phi}_f/\overline{T_e}$ and $\tilde{I}_{i,sat}/\overline{I}_{i,sat}$, quite different from the ZF. The cross-phase analysis suggests that the EO has finite poloidal and radial wave numbers and propagates in the ion diamagnetic drift direction. In this manuscript, we discriminate the ZF from the EO in the radial location $r < 4.5$ cm ($r = 4.5$ is a marginal location), and topics are limited on the ZF measured inside main plasmas. Furthermore, we can see a coherent fluctuation at 3 kHz. We denote the coherent fluctuations as the TM (the third mode). While the appearance and frequency of the TM change transiently during a single discharge, frequencies of the DW and ZF are

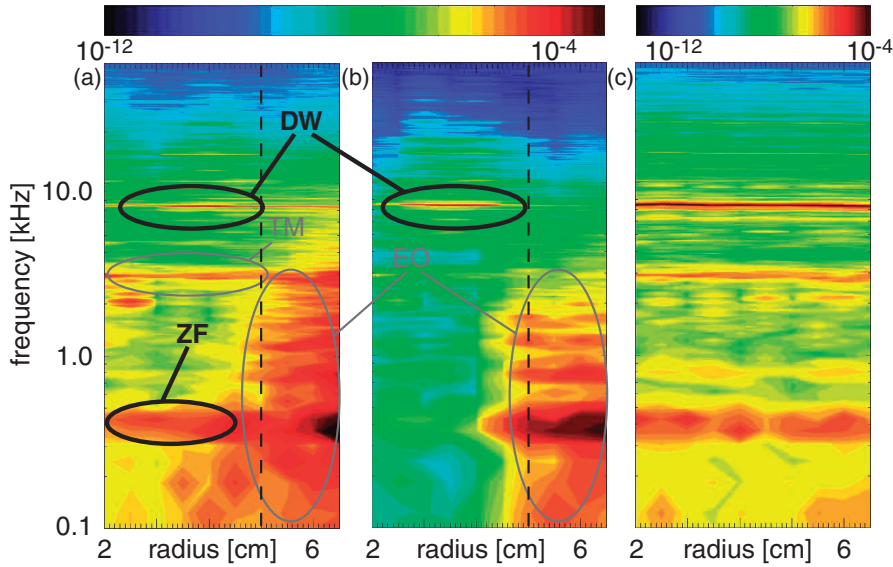


Fig. 2. Radial profiles of normalized auto-power spectra measured by shot-to-shot radial scan of the RSP. (a) Φ_f/\bar{T}_e , (b) $\bar{I}_{i,sat}/\bar{I}_{i,sat}$, and (c) Φ_f (arb. unit) measured with a reference probe during the shot-to-shot scan. Horizontal or vertical axis indicates radial location (linear scale) or frequency (logarithmic scale), and normalized powers are shown in color. In (c), the reference probe is fixed at $r = 4$ cm and the horizontal axis indicates the RSP location. In terms of frequency and radial location, four types of fluctuation are labeled as DW, ZF (in black), TM, and EO (in gray). Dashed vertical lines in (a) and (b) indicate the boundary of plasmas ($r = 5$ cm).

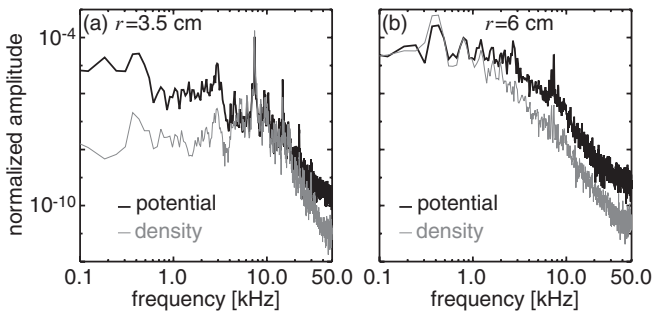


Fig. 3. Slices of auto-power spectra of Φ_f/\bar{T}_e (black) and $\bar{I}_{i,sat}/\bar{I}_{i,sat}$ (gray). (a) Measured at $r = 3.5$ cm; (b) Measured at $r = 6$ cm.

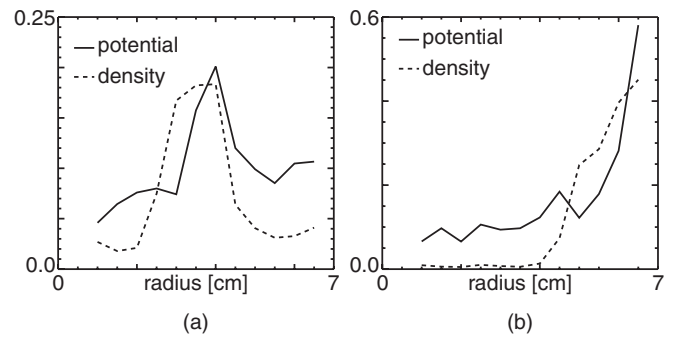


Fig. 4. Radial profiles of Φ_f/\bar{T}_e (solid) and $\bar{I}_{i,sat}/\bar{I}_{i,sat}$ (dashed). (a) DW (4–10 kHz); (b) ZF (0.3–0.5 kHz).

almost stationary (a gradual increase with time). Changes in TM frequency are correlated with transient behaviors of plasmas, and topics of the TM will be presented in a forthcoming article.

4. Particular Topics of Observed Fluctuations

In this section, differences between the DW and the ZF and specific features in each fluctuation are presented.

4.1 Slices of normalized auto-power spectra

We show slices of normalized auto-power spectra in order to compare normalized fluctuation amplitudes between Φ_f/\bar{T}_e and $\bar{I}_{i,sat}/\bar{I}_{i,sat}$ in detail. Figure 3(a) shows normalized auto-power spectra Φ_f/\bar{T}_e and $\bar{I}_{i,sat}/\bar{I}_{i,sat}$ at the radial position $r = 3.5$ cm [where the density gradient scale is short, as shown in Fig. 5(b)]. Comparing auto-powers, the fluctuation in the range of 4–20 kHz holds $\Phi_f/\bar{T}_e \sim \bar{I}_{i,sat}/\bar{I}_{i,sat}$. A spectral peak of the DW is observed at 7–8 kHz (the fundamental mode) as well as its higher harmonics. The fluctuation with a frequency lower than 4 kHz holds $\Phi_f/\bar{T}_e > \bar{I}_{i,sat}/\bar{I}_{i,sat}$. In particular, the mode at about 0.4 kHz has another spectral peak and a condition of

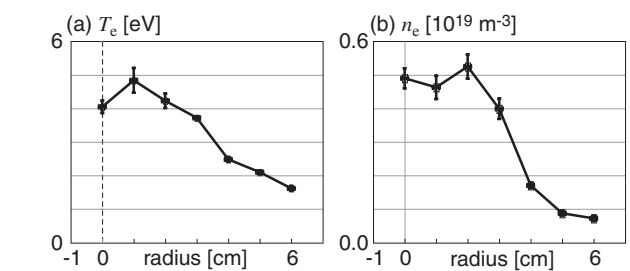


Fig. 5. Equilibrium radial profiles of the (a) electron temperature T_e (eV) and (b) electron density n_e (10^{19} m^{-3}).

$\Phi_f/\bar{T}_e \gg \bar{I}_{i,sat}/\bar{I}_{i,sat}$ (the ZF). Spectra at the radial position $r = 6$ cm (outside main plasmas) in Fig. 3(b) also show peaks at the ZF and the DW frequencies. However, the relationship between Φ_f/\bar{T}_e and $\bar{I}_{i,sat}/\bar{I}_{i,sat}$ at $r = 6$ cm is different from that at $r = 3.5$ cm. At the ZF frequency, Φ_f/\bar{T}_e becomes smaller than $\bar{I}_{i,sat}/\bar{I}_{i,sat}$, which is not consistent with the zonal flow. This fluctuation is the EO. Meanwhile, Φ_f/\bar{T}_e becomes larger than $\bar{I}_{i,sat}/\bar{I}_{i,sat}$ at the DW

frequency, which is not consistent with the linearly excited drift-wave.

Next, Fig. 4 shows radial profiles of the normalized fluctuation amplitudes of the DW (integrated in 4–10 kHz) and ZF (integrated in 0.3–0.5 kHz). The $\tilde{I}_{i,\text{sat}}/\bar{I}_{i,\text{sat}}$ of the DW has a maximum at the radial location $r = 3\text{--}4$ cm near the steep density gradient region [Fig. 5(b)] and values larger than 0.05 at $r = 2\text{--}5$ cm. $\tilde{\Phi}_f/\bar{T}_e \sim \tilde{I}_{i,\text{sat}}/\bar{I}_{i,\text{sat}}$ at $r = 3.5\text{--}4$ cm. The cross-phase analysis between the density and the potential at the maximal fluctuation amplitude shows a phase shift of ~ 0.028 ($\sim 10^\circ$) in typical turbulence spectra. The relationship is consistent with previous observations.^{3,5,6} The drift-wave holds the Boltzmann relationship between potential and density, and is excited in the steep density gradient region. Therefore, the DW has features of the drift-wave. In contrast to the DW, the $\tilde{\Phi}_f/\bar{T}_e$ of the ZF has ~ 0.1 at $r < 4.5$ cm ($\tilde{I}_{i,\text{sat}}/\bar{I}_{i,\text{sat}} \ll \tilde{\Phi}_f/\bar{T}_e$), which does not contradict the zonal flow feature.

4.2 Poloidal and axial structures of fluctuations

The zonal flow has poloidally and axially symmetric spatial structures. On the other hand, the drift-wave has finite poloidal and axial wave numbers. We investigate the spatial structures of the fluctuations by cross-correlation analysis. Figures 6 and 7 show poloidal and axial cross-phases of the ZF and DW [measured poloidal angles are from -0.0194 to 0.73 in $\text{rad}/(2\pi)$, and measured axial distances are $15\text{--}90$ cm]. The statistical significance is shown as the squared cross-coherence. Poloidal cross-phases were measured at the radial location $r = 4$ cm and axial location $z = 90$ cm, based on a reference probe at the same poloidal plane. Axial cross-phases were measured at the same radial location. The cross-phases of the ZF are within ± 0.2 and consistent with the poloidal mode $m = 0$ and axial mode $n = 0$, where $n = 1$ indicates the axial wavelength is the same as the vessel length. On the other hand, the DW propagates in the electron diamagnetic drift direction with $m = 3\text{--}5$ and $n = 2\text{--}3$. (We also measured the cross-phase of the DW between two probes within 2.5 cm poloidal and 2.5 cm axial distances. After removing the effect of the poloidal cross-phase, the axial cross-phase of the 2.5 cm axial distance is less than $0.1 \text{ rad}/(2\pi)$.) These results confirm that the ZF or DW has poloidal and axial structures consistent with the zonal flow or drift-wave, respectively.

4.3 Radial structures of fluctuations and velocity fluctuation correlated with the ZF

The zonal flow appears as a radial electric field oscillation and has a finite radial wave number of potential oscillation. Therefore, information on radial wave number is necessary for identifying the zonal flow. The drift-wave can also have a finite radial wave number in its dispersion relation $f_{\text{DW,th}} = \omega_e^*/[2\pi(1 + k_\perp^2 \rho_s^2)]$ derived from the Charney–Hasegawa–Mima equation,³⁰ where $\omega^* = k_\theta T_e/(eB\lambda_n)$ is the electron drift frequency, k_θ is the poloidal wave number of the drift-wave, and λ_n is the density gradient scale length.

Figure 8(a) shows the radial profile of k_r of the ZF. The ZF has finite radial wave numbers at the radial locations $r \sim 2$ and 4 cm. However, we also observe an inversion of polarity in the ZF k_r relative to the location of maximal DW amplitude. This observation shows a shear structure of k_r ,

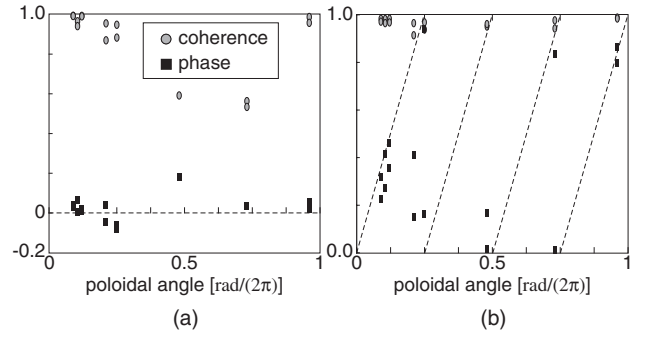


Fig. 6. Results from poloidal correlation analysis measured at $r = 4$ cm. Squared cross-coherence and cross-phase ($\text{rad}/2\pi$) of the (a) ZF and (b) DW. Dashed lines indicate $m = 0$ (a) and 4 (b). The significance level is 0.0625.

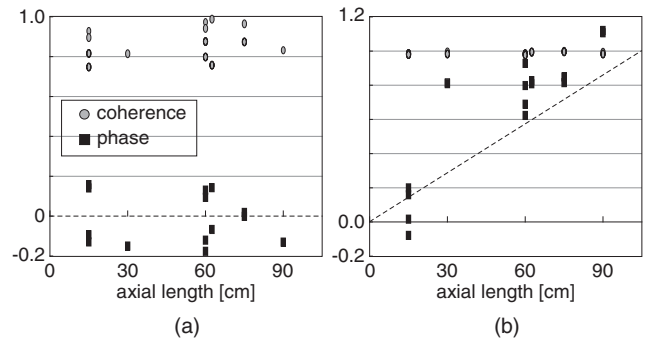


Fig. 7. Results from axial correlation analysis at $r = 4$ cm. Squared cross-coherence and cross-phase ($\text{rad}/2\pi$) of the (a) ZF and (b) DW. Dashed lines indicate $n = 0$ (a) and 2 (b), where $n = 1$ shows that axial wavelength is the same as vessel length. The significance level is 0.0625.

and can be discriminated from both uniform potential oscillations and a single-mode zonal flow. Uniform potential oscillations have a zero k_r and are not the zonal flow. Propagating zonal flows have a finite k_r with a uniform sign. The observed k_r profile indicates a curvature of potential (sheared radial electric field). On the other hand, Fig. 8(b) shows the radial profile of k_r of the DW. Signs of the k_r polarity change radially, indicating that the k_r of the DW is modulated spatially (vortex tilting). The radial k_r modulation can generate a stationary turbulence Reynolds stress. Figure 8(c) demonstrates radial profile of the turbulence Reynolds stress per mass density. At radial locations where signs of the k_r polarity change, steep Reynolds stress gradients are formed, suggesting the generation of a stationary zonal flow. However, the TDE analysis does not reveal the stationary shear flow in this experiment. Results of the stationary flow should be given by measurement with a higher precision, and thus we do not make any conclusion regarding the stationary zonal flow in this manuscript.

The zonal flow in reality is a sheared poloidal flow (sometimes including a parallel flow). The ZF oscillates at ~ 0.4 kHz in this experiment; therefore, if the ZF is the zonal flow, the ZF should be associated with a poloidal velocity oscillation. In the radial location where the k_r of the ZF has a finite value, a spectral peak of \tilde{V}_θ at the ZF frequency is observed by TDE analysis, as shown in Fig. 9(a) (at $r = 2.5$ cm in this case). A time window of $512 \mu\text{sec}$ (longer than the $\tau_{\text{min,fluctuations}}$ of $7\text{--}8$ kHz DW and shorter than the

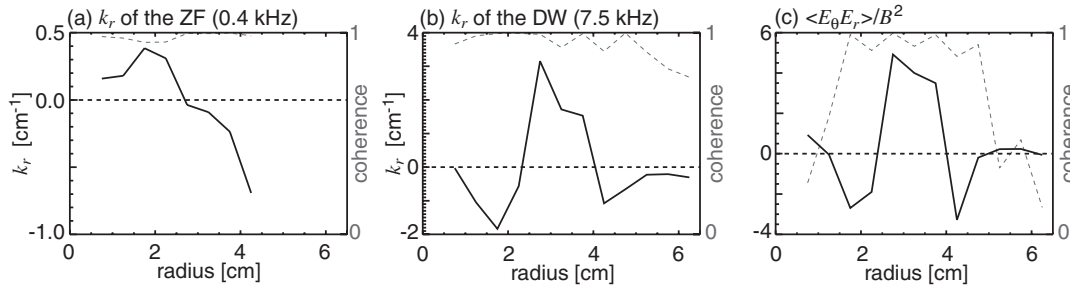


Fig. 8. Radial wave numbers of the (a) ZF and (b) DW. (c) Turbulence Reynolds stress per mass density. The significance level is 0.0625.

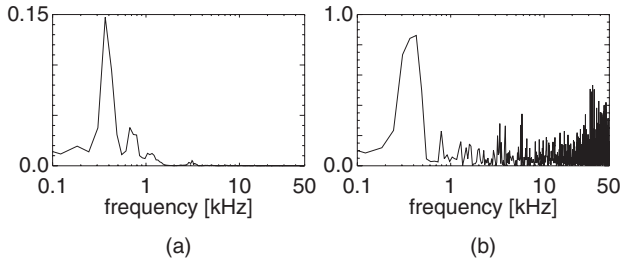


Fig. 9. (a) Auto-power spectrum of poloidal velocity fluctuation \tilde{V}_θ measured at $r = 2.5$ cm. (b) Squared cross-coherence between \tilde{V}_θ and $\tilde{\Phi}_f$.

τ_{flows} of 0.3 kHz ZF) was used in the time-resolved cross-correlation analysis. The \tilde{V}_θ at the ZF frequency has a significantly high coherence with the potential oscillation in Fig. 9(b), confirming that the ZF is associated with a poloidal flow oscillation.

4.4 Linear dispersion relation of the DW

We compare the observed and theoretically estimated DW frequencies. Not considering the effect of the Doppler shift, the drift-wave frequency is $f_{\text{DW,th}}$. We calculate $f_{\text{DW,th}}$ at $r \sim 3.5$ cm, where the radial distribution of $\tilde{I}_{i,\text{sat}}/\bar{I}_{i,\text{sat}}$ has a maximum at $r = 3-4$ cm. The experimental parameters $m = 3-5$, $T_e = 3.1$ eV [Fig. 5(a)], $\lambda_n = 1.3$ cm [Fig. 5(b)], and $k_r = 1.8 \text{ cm}^{-1}$ [Fig. 8(b)] are used, and $f_{\text{DW,th}} = 6.22-8.26$ kHz is obtained, which is consistent with the observed peak frequency of 7–8 kHz. The plasma potential profile can be extrapolated from the electron temperature and floating potential. We obtained the effect of the Doppler shift by the radial electric field $\omega_{\mathbf{E} \times \mathbf{B}}/(2\pi)$, and the ratio of $\omega_{\mathbf{E} \times \mathbf{B}}/(2\pi)$ to the electron diamagnetic drift frequency ω_{*e} is $\sim 1/3$. However, the validity of the extrapolation and precise measurement of the Doppler shift should be investigated in future studies.

In addition, we also present results for the linear dispersion relation and most unstable modes from the numerical linear device code (NLD).³¹⁾ The NLD includes three fluctuation parameters, potential, density, and parallel velocity, as well as the effect of ion-neutral collision. Figure 10 shows results from the NLD under the same equilibrium conditions in Fig. 5. Fluctuations with $m = 3-7$ are unstable and have a maximal growth rate at $m = 4$. This is consistent with the result for the observed DW with $m = 3-5$. However, frequencies from the NLD are higher than the observed values. Here, frequencies of the DW are calculated without the effect of the Doppler shift by stationary plasma flows. The precise identification of the

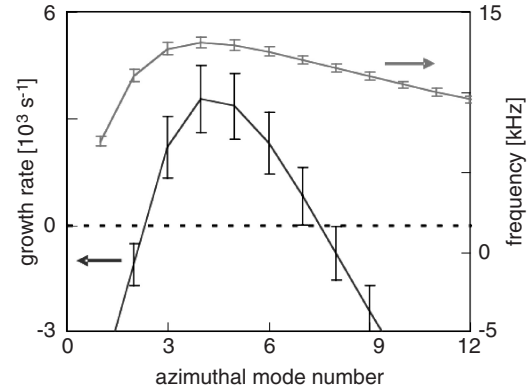


Fig. 10. Results from numerical linear device code. Growth rates and real frequencies versus azimuthal mode number are shown. Fluctuations with $m = 3-7$ are unstable.

drift-wave frequency involves the consideration of the Doppler shift and should be performed as a future work.

4.5 Nonlinear interaction between the ZF and the DW

The zonal flow is considered to be excited nonlinearly by turbulence. The nonlinear interaction can be tested by cross-correlation analysis between the zonal flow and the envelope of the drift-wave turbulence.³²⁻³⁴⁾ Figure 11 shows evidence of the nonlinear interaction between the ZF and the DW. To optimize statistics, the spectra are averaged over a 0.1–0.37 span range during a discharge. The power spectrum of the original $\tilde{\Phi}_f$ given in Fig. 11(a) has two distinctive spectral peaks corresponding to the ZF and DW. Another power spectrum shown in Fig. 11(b) indicates the envelope of $\tilde{\Phi}_f$ in the frequency range of 6.5–7.5 kHz (the DW). A spectral peak at the ZF frequency demonstrates that the DW envelope is modulated at the ZF frequency. Figure 11(c) shows the squared cross-coherence between the ZF and the envelope of the DW. A significant peak at the ZF frequency indicates that the nonlinear relationship between the ZF and the DW is statistically significant.

The bispectral analysis also demonstrate a significance of nonlinear three-wave interaction,³⁵⁾ and is applied to the nonlinear interaction between the zonal flow (geodesic acoustic mode¹⁶⁾) and turbulence.³⁶⁻⁴⁰⁾ Figure 12 shows the auto-bicoherence plot of the floating potential fluctuations, normalized $(\tilde{\Phi}_f(f_1)\tilde{\Phi}_f(f_3 - f_1)\tilde{\Phi}_f^*(f_3))$, at frequency $3 = 0.366$ kHz (frequency of the ZF). A significant spectral peak at $f_1 \sim 7-8$ kHz confirms that the ZF is nonlinearly coupled to the DW.

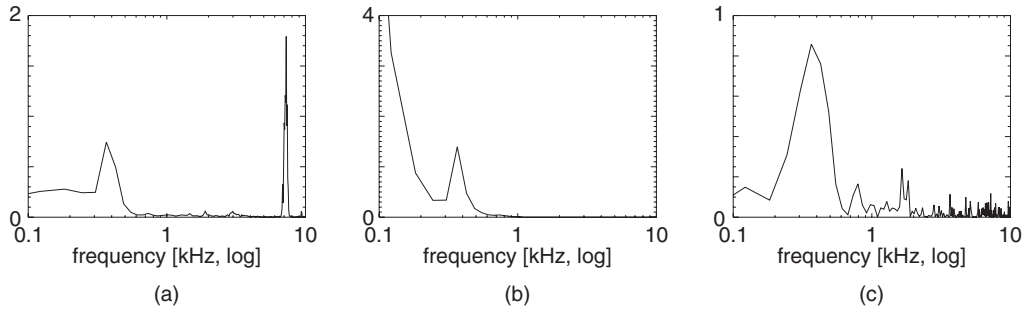


Fig. 11. Amplitude modulation of the DW synchronized at the ZF oscillation measured at $r = 3.25\text{--}3.5$ cm (SN 5716, 0.1–0.37 s average). (a) Auto-power of original Φ_f , (b) auto-power of the envelope of Φ_f in 6.5–7.5 kHz frequency range. A linear scale is chosen in the vertical axis. (c) Squared cross-coherence between original and envelope waves.

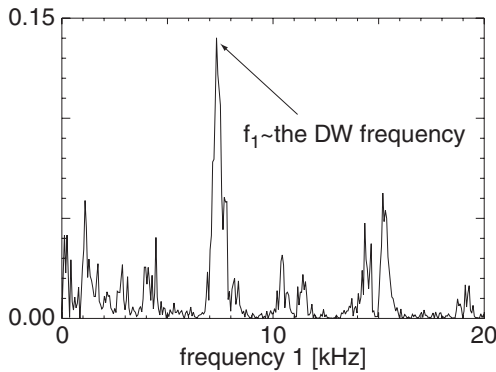


Fig. 12. Auto-bicoherence of floating potential fluctuation at frequency 3 = 0.366 kHz (frequency of the ZF). The horizontal axis indicates frequency 1. The significance level is ~ 0.002 .

5. Discussion and Summary

In this observation, the ZF has many features consistent with the zonal flow. However, the shear structure of the ZF cannot be simply understood. Theories show that the zonal flow is an electrostatic potential with a finite radial wave number. This is based on a picture that the zonal flow is a “mode”. In terms of the “mode” problem, the observation shows the coexistence of two “modes” of the ZF with the same frequency. The two modes have opposite signs of the radial wave number relative to the radial location where the DW has a maximal fluctuation amplitude. This observation is different from the conventional picture of the parametric-modulational interaction among four waves (primary drift-wave, two sidebands of the primary drift-wave, and a zonal flow). We may interpret the observation using the vorticity equation. On the basis of the vorticity equation $\partial_t \Delta \Phi_{ZF}/B = \partial_{rr}(\langle \tilde{E}_\theta \tilde{E}_r \rangle / B^2) - \mu \Delta \Phi_{ZF}/B$, zonal flow vorticity can be driven by a curvature of turbulence Reynolds stress. We assume the condition that the Reynolds stress has purely oscillating components (no stationary Reynolds stress). When the amplitude of the turbulence Reynolds stress curvature becomes larger than the damping rate of the zonal flow vorticity at a location, the profile of the turbulent Reynolds stress has two steep gradient regions, which are distributed symmetrically with opposite signs, resulting in excitation of the two zonal flow “modes”. In this observation, however, there is a stationary turbulence Reynolds stress (gradient) per mass density. Therefore, the observation may be interpreted by a picture of a limit cycle. Oscillating

turbulence Reynolds stress assists the excitation of the stationary zonal flow in the region where the Reynolds stress has a steep gradient. This can realize an “oscillating” zonal flow, but in reality, there is merely a bistable transition in which a stationary zonal flow is accelerated or decelerated. For further study, we need a precise poloidal flow velocity measurement by which we make a conclusion regarding the relationship between stationary zonal flow and stationary Reynolds stress and their dynamical behaviors.

In summary, we investigated low frequency fluctuations in the large mirror device. We found the coexistence of two distinctive modes at frequencies of 0.3–0.5 kHz (ZF) and 6–8 kHz (DW). The ZF is located at $r < 4.5$ cm at least and has $m/n \sim 0$ and a radial shear structure (curvature of potential), associated with poloidal velocity fluctuations. The DW has a maximal amplitude in the steep density gradient region, $m/n = 3\text{--}5/2\text{--}3$, and finite radial wave numbers. The radial wave number of the drift-wave changes in radius, indicating vortex tilting. Linear properties of the DW do not contradict theoretical and simulation results. The nonlinear interaction between the ZF and the DW is confirmed by envelope and bispectral analyses. The ZF or DW is identified as the residual zonal flow or drift-wave, respectively.

Acknowledgments

We are grateful to Professors T. Ohkawa and F. Wagner for useful discussions. This work was partially supported by a Grant-in-Aid for Specially-Promoted Research (16002005) [Itoh Project] and a Grant-in-Aid for Young Scientists (B) (18760637) from the Ministry of Education, Culture, Sports, Science and Technology. This work was also partially supported by the collaborations of National Institute for Fusion Science (NIFS07KOAP017) and of Research Institute for Applied Mechanics, Kyushu University. We also appreciate the experimental support given by Mr. T. Nishijima, Mr. M. Kawaguchi, Mr. K. Kamataki, Mr. T. Maruta, Kawai laboratory and Tanaka laboratory in the Interdisciplinary Graduate School of Engineering Science, Kyushu University.

- 1) W. Horton: *Rev. Mod. Phys.* **71** (1999) 735.
- 2) H. Hendel, T. Chu, and P. Politzer: *Phys. Fluids* **11** (1968) 2426.
- 3) D. Jassby: *Phys. Fluids* **15** (1972) 1590.
- 4) H. Pecseli, T. Mikkelsen, and S. Larsen: *Plasma Phys.* **25** (1983) 1173.
- 5) A. Komori and N. Sato: *Jpn. J. Appl. Phys.* **23** (1984) 475.

- 6) Y. Suetsugu, A. Komori, and Y. Kawai: *J. Phys. Soc. Jpn.* **54** (1985) 3664.
- 7) A. K. Sen, J. Chen, and M. Mael: *Phys. Rev. Lett.* **66** (1991) 429.
- 8) T. Klinger, A. Latten, A. Piel, G. Bonhomme, T. Pierre, and T. Dudok de Wit: *Phys. Rev. Lett.* **79** (1997) 3913.
- 9) T. Kaneko, H. Tsunoyama, and R. Hatakeyama: *Phys. Rev. Lett.* **90** (2003) 125001.
- 10) O. Grulke, S. Ullrich, T. Windisch, and T. Klinger: *Plasma Phys. Control. Fusion* **49** (2007) B247.
- 11) G. R. Tynan, M. Burin, C. Holland, G. Antar, N. Crocker, and P. H. Diamond: *Phys. Plasmas* **11** (2004) 5195.
- 12) M. Burin, G. R. Tynan, G. Antar, N. Crocker, and C. Holland: *Phys. Plasmas* **12** (2005) 052320.
- 13) F. Poli, S. Brunner, A. Diallo, A. Fasoli, I. Furno, B. Labit, S. H. Müller, G. Plyushchev, and M. Podestà: *Phys. Plasmas* **13** (2006) 102104.
- 14) P. H. Diamond, S.-I. Itoh, K. Itoh, and T. S. Hahm: *Plasma Phys. Control. Fusion* **47** (2005) R35.
- 15) M. N. Rosenbluth and F. L. Hinton: *Phys. Rev. Lett.* **80** (1998) 724.
- 16) N. Winsor, J. Johnson, and J. Dawson: *Phys. Fluids* **11** (1968) 2448.
- 17) Z. Lin, T. S. Hahm, W. W. Lee, W. M. Tang, and R. B. White: *Science* **281** (1998) 1835.
- 18) P. H. Diamond, M. N. Rosenbluth, E. Sanchez, C. Hidalgo, B. Van Milligen, T. Estrada, B. Brañas, M. Hirsch, H. J. Hartfuss, and B. A. Carreras: *Phys. Rev. Lett.* **84** (2000) 4842.
- 19) G. R. Tynan, R. A. Moyer, M. J. Burin, and C. Holland: *Phys. Plasmas* **8** (2001) 2691.
- 20) A. Fujisawa, K. Itoh, H. Iguchi, K. Matsuoka, S. Okamura, A. Shimizu, T. Minami, Y. Yoshimura, K. Nagaoka, C. Takahashi, M. Kojima, H. Nakano, S. Ohsima, S. Nishimura, M. Isobe, C. Suzuki, T. Akiyama, K. Ida, K. Toi, S.-I. Itoh, and P. H. Diamond: *Phys. Rev. Lett.* **93** (2004) 165002.
- 21) A. Fujisawa, A. Shimizu, H. Nakano, S. Ohshima, K. Itoh, Y. Nagashima, S.-I. Itoh, H. Iguchi, Y. Yoshimura, T. Minami, K. Nagaoka, C. Takahashi, M. Kojima, S. Nishimura, M. Isobe, C. Suzuki, T. Akiyama, T. Ido, K. Matsuoka, S. Okamura, and P. H. Diamond: *Plasma Phys. Control. Fusion* **49** (2007) 211.
- 22) A. Fujisawa, A. Shimizu, H. Nakano, S. Ohshima, K. Itoh, Y. Nagashima, S.-I. Itoh, H. Iguchi, Y. Yoshimura, T. Minami, K. Nagaoka, C. Takahashi, M. Kojima, S. Nishimura, M. Isobe, C. Suzuki, T. Akiyama, T. Ido, K. Matsuoka, S. Okamura, and P. H. Diamond: *J. Phys. Soc. Jpn.* **76** (2007) 033501.
- 23) H. Xia and M. Shats: *Phys. Rev. Lett.* **91** (2003) 155001.
- 24) M. Shats, W. Solomon, and H. Xia: *Phys. Rev. Lett.* **90** (2003) 125002.
- 25) D. K. Gupta, R. J. Fonck, G. R. McKee, D. J. Schlossberg, and M. W. Shafer: *Phys. Rev. Lett.* **97** (2006) 125002.
- 26) A. Fujisawa, K. Itoh, A. Shimizu, H. Nakano, S. Ohshima, H. Iguchi, K. Matsuoka, S. Okamura, T. Minami, Y. Yoshimura, K. Nagaoka, K. Ida, K. Toi, C. Takahashi, M. Kojima, S. Nishimura, M. Isobe, C. Suzuki, T. Akiyama, Y. Nagashima, S.-I. Itoh, and P. H. Diamond: *Phys. Rev. Lett.* **98** (2007) 165001.
- 27) C. Holland, J. H. Yu, A. James, D. Nishijima, M. Shimada, N. Taheri, and G. R. Tynan: *Phys. Rev. Lett.* **96** (2006) 195002.
- 28) V. Sokolov, X. Wei, A. K. Sen, and K. Avinash: *Plasma Phys. Control. Fusion* **48** (2006) S111.
- 29) Y. Saitou, A. Yonesu, S. Shinohara, M. V. Ignatenko, N. Kasuya, M. Kawaguchi, K. Terasaka, T. Nishijima, Y. Nagashima, Y. Kawai, M. Yagi, S.-I. Itoh, M. Azumi, and K. Itoh: *Phys. Plasmas* **14** (2007) 072301.
- 30) A. Hasegawa and K. Mima: *Phys. Rev. Lett.* **39** (1977) 205.
- 31) N. Kasuya, M. Yagi, M. Azumi, K. Itoh, and S.-I. Itoh: *J. Phys. Soc. Jpn.* **76** (2007) 044501.
- 32) G. R. McKee, R. J. Fonck, M. Jakubowski, K. H. Burrell, K. Hallatschek, R. A. Moyer, D. L. Rudakov, W. Nevins, G. D. Porter, P. Schoch, and X. Xu: *Phys. Plasmas* **10** (2003) 1712.
- 33) T. Ido, Y. Miura, K. Hoshino, K. Kamiya, Y. Hamada, A. Nishizawa, Y. Kawasumi, H. Ogawa, Y. Nagashima, K. Shinohara, Y. Kusama, and JFT-2M group: *Nucl. Fusion* **46** (2006) 512.
- 34) Y. Nagashima, K. Itoh, S.-I. Itoh, A. Fujisawa, M. Yagi, K. Hoshino, K. Shinohara, A. Ejiri, Y. Takase, T. Ido, K. Uehara, Y. Miura, and the JFT-2M group: *Plasma Phys. Control. Fusion* **49** (2007) 1611.
- 35) Y. Kim and E. Powers: *IEEE Trans. Plasma Sci.* **7** (1979) 120.
- 36) M. G. Shats and W. M. Solomon: *Phys. Rev. Lett.* **88** (2002) 045001.
- 37) G. S. Xu, B. N. Wan, and M. Song: *Phys. Plasmas* **9** (2002) 150.
- 38) Y. Nagashima, K. Hoshino, A. Ejiri, K. Shinohara, Y. Takase, K. Tsuzuki, K. Uehara, H. Kawashima, H. Ogawa, T. Ido, Y. Kusama, and Y. Miura: *Phys. Rev. Lett.* **95** (2005) 095002.
- 39) K. J. Zhao, T. Lan, J. Q. Dong, L. W. Yan, W. Y. Hong, C. X. Yu, A. D. Liu, J. Qian, J. Cheng, D. L. Yu, Q. W. Yang, X. T. Ding, Y. Liu, and C. H. Pan: *Phys. Rev. Lett.* **96** (2006) 255004.
- 40) C. Holland, G. R. Tynan, R. J. Fonck, G. R. McKee, J. Candy, and R. E. Waltz: *Phys. Plasmas* **14** (2007) 056112.